Supplemental Information

Acquisition of MRI data

Sixty-four gradient-weighted volumes were acquired using a spin-echo echoplanar imaging (EPI) sequence with the following parameters: *b*-value, 1000 s/mm^2; 65 consecutive axial slices of thickness 2.4 mm; 104 × 104 image matrix with an in-plane voxel resolution of 2.4 × 2.4 mm; field of view, 25 × 25 cm; repetition time, 8.4 s; echo time, 88 ms; flip angle, 90°. Additionally, a separate T_2-weighted (i.e. *b* = 0) volume was acquired before acquisition of the diffusion-weighted volumes. Gradient directions were isotropically distributed on the half-sphere. Head movement and artifacts attributable to eddy currents were corrected using FSL software. Gradient directions were not adjusted to account for slight rotations of the gradient-weighted volumes performed to correct for head movement. The mean signal-to-noise ratio (SNR) of the diffusion-weighted images was 28.3 ± 0.7, where the standard deviation was computed over all diffusion weighted images. Subjects were imaged in no particular order. To serve as a quality control measure, the amount of head rotation between the initial reference volume (no gradient weighting) and each of the 64 subsequent gradient-encoded volumes was estimated from the rotation matrices computed to correct for head movement. These 64 estimates of head rotation were averaged for each subject to yield an average estimate of head rotation. The average estimate of head rotation was not different between controls and patients (rotation patients: 0.6 ± 0.4°, rotation controls: 0.7 ± 0.3°, d.f. = 104, *t* = 1.0, *p* = 0.31).

Whole-brain tractography

Any voxel with fractional anisotropy exceeding a predefined threshold (0.3) was classified as white-matter. For each voxel classified as white-matter, a streamline was initialized from the two opposing directions of the principal eigenvector. Each streamline was propagated using the FACT algorithm (1,2). Propagation was terminated if either a minimum angle threshold of 50° was violated or if a voxel was encountered with fractional anisotropy (FA) below 0.2. At each increment, the direction of propagation was parallel to the orientation of the eigenvector closest to the current streamline endpoint. The two opposing streamlines initialized from each voxel were then joined at their point of initialization to yield a single streamline. Each streamline was normalized to MNI space using the nonlinear warp computed during the preprocessing stage. This resulted in a whole-brain tractographic map in MNI space for each subject comprising a

total of 56114 ± 6245 streamlines, where the standard deviation was computed over all subjects. Tractographic maps were viewed with the TrackVis software (http://www.trackvis.org).

Note that streamline tractography introduces two distinct kinds of distal bias. The first kind of bias gives rise to a positive association between the number of streamlines interconnecting a pair of nodes and the distance by which the pair is separated. This "positive" bias arises due to the fact that a longer fiber bundle encompasses a greater number of white-matter voxels, and thus implies a greater number of streamlines are seeded in comparison to a shorter fiber bundle. The second kind of bias gives rise to a negative association between the number of streamlines interconnecting a pair of nodes and the distance by which the pair is separated. This "negative" bias arises due to the fact that a longer streamline must undergo a greater number of forward propagations. At each forward propagation, there is a chance that the streamline is steered off course due to a noisy estimate of the local propagation direction. Given that a longer streamline undergoes a greater number of forward propagations, the risk of a streamline being steered off course increases with its length. It is not clear if these two kinds of bias cancel each other out.

Fiber tract network model

Grey-matter nodes were defined using the automated anatomical labeling (AAL) parcellation atlas (3). Subcortical and cerebellum nodes were omitted, resulting in a total of 82 cortical nodes exclusively modeling cortico-cortical connectivity. The corticospinal tracts and cortico-subcortical connectivity was not modeled.

The tractographic maps were utilized to determine if a pair of nodes was connected via a link in the graph model. Specifically, an 82 × 82 connectivity matrix, denoted as **A** herein, was populated for each subject. To populate **A**, only streamlines with endpoints residing in different nodes were considered. Streamlines with both endpoints in the same node (self-loops), or streamlines with at least one endpoint residing in white-matter, the cerebellum or a subcortical structure were given no further consideration. For example, if a streamline was terminated before entering a node, due to encountering a voxel with FA below 0.2 or violating a minimum angle threshold of 50°, then that streamline was discarded and given no further consideration. Fiber bundles were considered linked to a node if one of the fiber bundle's endpoints resided within that node (4). Similar procedures have been implemented elsewhere, for example, as in (4). Any streamline of length less than 20 mm was considered spurious and also given no further consideration. Note that while a genuine fiber may be less than 20 mm in length and thereby excluded by this threshold, opting for a conservative threshold ensures elimination of all

spurious streamlines, since it is unlikely that a spurious streamline can propagate for more than 20 mm. The set of remaining streamlines therefore exclusively characterized cortico-cortical connections. Streamlines were significantly longer in controls (length patients: 4.7 ± 0.3 cm, length controls: 4.9 ± 0.3 cm, t = 2.7, p = 0.009). The total number of *all* streamlines (i.e. inclusive of streamlines less than 20 mm) was not significantly different between groups.

To define an undirected and unweighted graph, the connectivity matrix **A** was binarized with respect to a given threshold $T \geq 0$ to yield an adjacency matrix, denoted as **A'** herein. Specifically, $\mathbf{A}_{i,j} > T$ then $\mathbf{A'}_{i,j} = 1$, otherwise $\mathbf{A'}_{i,j} = 0$. Therefore, a link was drawn between two nodes if and only if they were connected via more than T streamlines. Graphs obtained over a range of binarizing thresholds that ensured full connectivity were considered.

Network attributes

Network organization was quantified in terms of nodal degree, efficiency, characteristic path length, clustering coefficient and small-worldness. These five attributes are defined and briefly discussed below. See (5-7) for further discussion.

The *degree* of a node is simply the number of links that connect it to other nodes of the network. Node degree is the most fundamental network measure and most other measures are ultimately linked to node degree (5).

The path length between two nodes is the minimum number of links that must be traversed to establish a connection (8). Unity path length indicates a pair of nodes is directly connected via a single link. The *characteristic path length* is the average path length across all possible node pairs. Characteristic path length was computed as the harmonic mean to sensibly deal with disconnected nodes (i.e. degree zero), which are of infinite path length (6). Note that path length is not related to the length of a streamline. *Efficiency* is simply the inverse of path length (9). Efficiency and path length are associated with how well a network supports parallel information transfer.

If the nearest neighbors of a node are also directly connected to each other they form a cluster. The *clustering coefficient* quantifies the number of links that exist between the nearest neighbors of a node as a proportion of the maximum number of possible connections (5,10). High clustering is associated with robustness to node deletion and local efficiency of information transfer.

A small-world network jointly supports efficient information transfer between distant nodes as well as nodes comprising local neighborhoods. While alternative models also offer efficient communication between distant nodes (i.e. randomly interconnected networks), they do not

jointly offer efficient local information transfer. The small-world network is therefore considered an attractive model for brain connectional architecture because it allows for both cortical integration (distant efficiency) as well as segregation (local efficiency).

A network is said to be small-world if it demonstrates greater clustering than a comparable random graph, but approximately the same characteristic path length. These requirements can be assessed quantitatively with the *small-world* ratio (σ-ratio) of normalized clustering to normalized path length, which is greater than unity for a small-world network. Clustering and path length were normalized with respect to 10^3 random graphs that were matched in the number of nodes and degree distribution. The rewiring algorithm of (11), was used to generate each degree-matched randomization.

Network-based statistic

The network-based statistic (NBS) is a network-based equivalent of the suprathreshold cluster-based test (12,13) used in traditional neuroimaging studies. Suprathreshold cluster-based tests threshold a statistic image using a predetermined primary threshold. The size of a connected suprathreshold cluster is then used to assess its significance. In particular, a corrected *p*-value for each suprathreshold cluster is calculated using the null distribution of the maximal suprathreshold cluster size. With the NBS, a suprathreshold cluster is analogous to a suprathreshold connected component, and thresholding is performed on network links rather than a statistic image.

The NBS was implemented in the present study as follows. A primary threshold was first applied to the *t*-statistic computed for each link to define a set of suprathreshold links. Any connected components in the set of suprathreshold links and their associated size (number of links) were then determined. The significance of a component was assessed based on its size. In particular, a corrected *p*-value was calculated for each component using the null distribution of maximal connected components. The null distribution was derived empirically using a nonparametric permutation approach. A total of 5000 randomized groupings of controls and patients were generated. For each of these randomized groupings (permutations), a parametric *t*-statistic was computed independently for each link and the size of the maximal connected component in the set of suprathreshold links was determined. A corrected *p*-value for a connected component of size *J* found in the non-randomized data was then determined by finding the proportion of the 5000 permutations for which the maximal connected component was larger than *J*.

Associations with intelligence quotient

A strong linear association was found in the control group between intelligence quotient and three key attributes of network organization; namely, global efficiency, path length and clustering coefficient. No such associations were found in the patient group (see Figure S2). The slope of the line (least squares fit) predicting each of these three attributes of network organization from intelligence quotient was tested for a difference between groups. Slopes were significantly different between controls and patients for all three attributes (Global efficiency: slope patients = 0.004 ± 0.01, slope controls = 0.05 ± 0.02, t = 2.1, p = 0.02; Path length: slope patients = -0.08 ± 0.58, slope controls = -1.92 ± 0.85, t = 1.8, p = 0.04; Clustering coefficient: slope patients = 0.005 ± 0.019, slope controls = 0.13 ± 0.034, t = 3.2, p = 0.001).

Alternative NBS parameter settings

To explore the sensitivity of the results to the NBS parameter settings, several alternative parameter combinations were investigated in an exploratory manner. As these secondary analyses were undertaken purely to examine the robustness of the findings to parameter settings, correction for multiple comparisons was not performed for each additional parameter combination investigated. Nodes comprising medial frontal and parietal/occipital regions were consistently observed for all parameter combinations considered. For some alternative parameter settings that still satisfied $p < 0.05$ corrected, the frontal subnetwork grew to include prefrontal nodes, and several nodes comprising the left temporal lobe emerged (see Figure S3). The NBS parameter settings used to generate Figure S3 were: K_{avg} = 1.5 and a streamline length threshold of 10 mm.
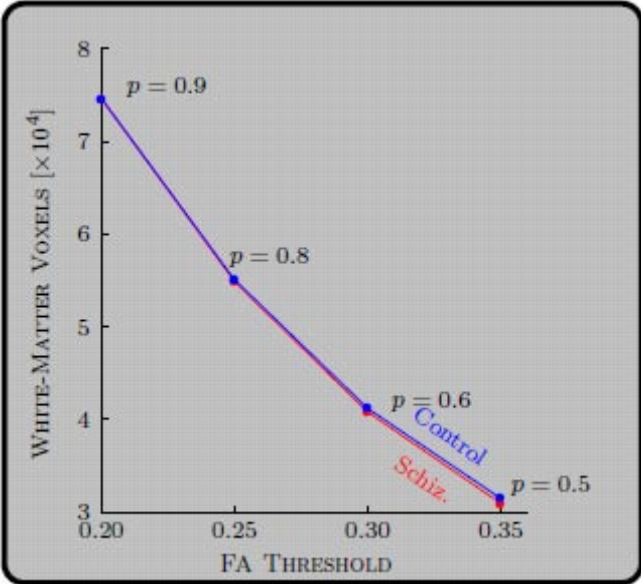
Figure S1. A voxel was classified as belonging to white-matter if its fractional anisotropy (FA) exceeded a predefined threshold. For all FA thresholds investigated, the number of voxels classified as white-matter was not significantly different between patients with schizophrenia and controls. A voxel was classified as belonging to white-matter if its fractional anisotropy exceeded a predefined threshold. For all FA thresholds investigated, the number of voxels classified as white-matter was not significantly different between patients with schizophrenia and controls.
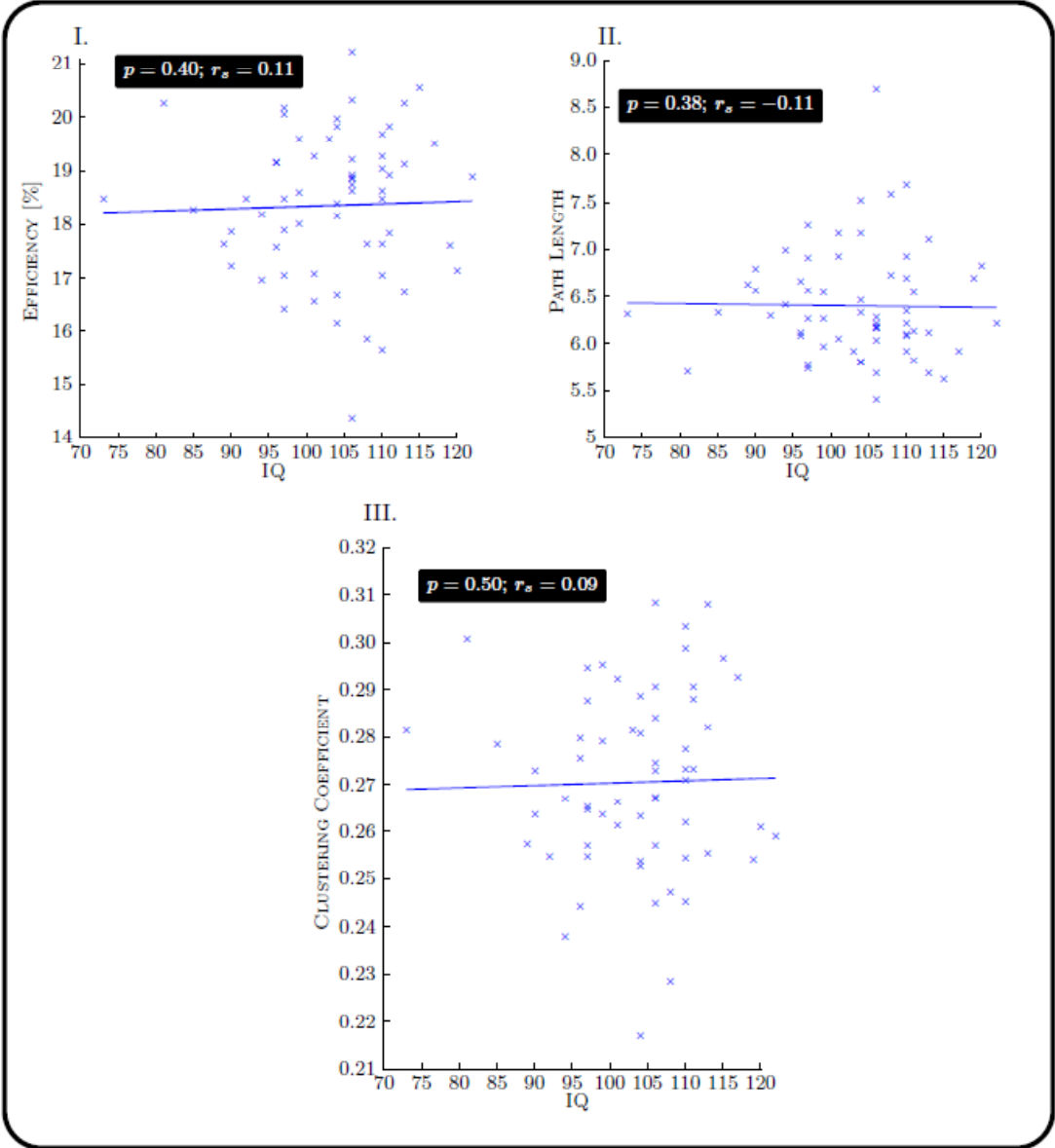
Figure S2. No linear association was found in the patient group between intelligence quotient (IQ), estimated using the Wechsler Test of Adult Reading (WTAR), and three attributes of network organization; namely, **I.** global efficiency, **II.** characteristic path length and **III.** average clustering coefficient.
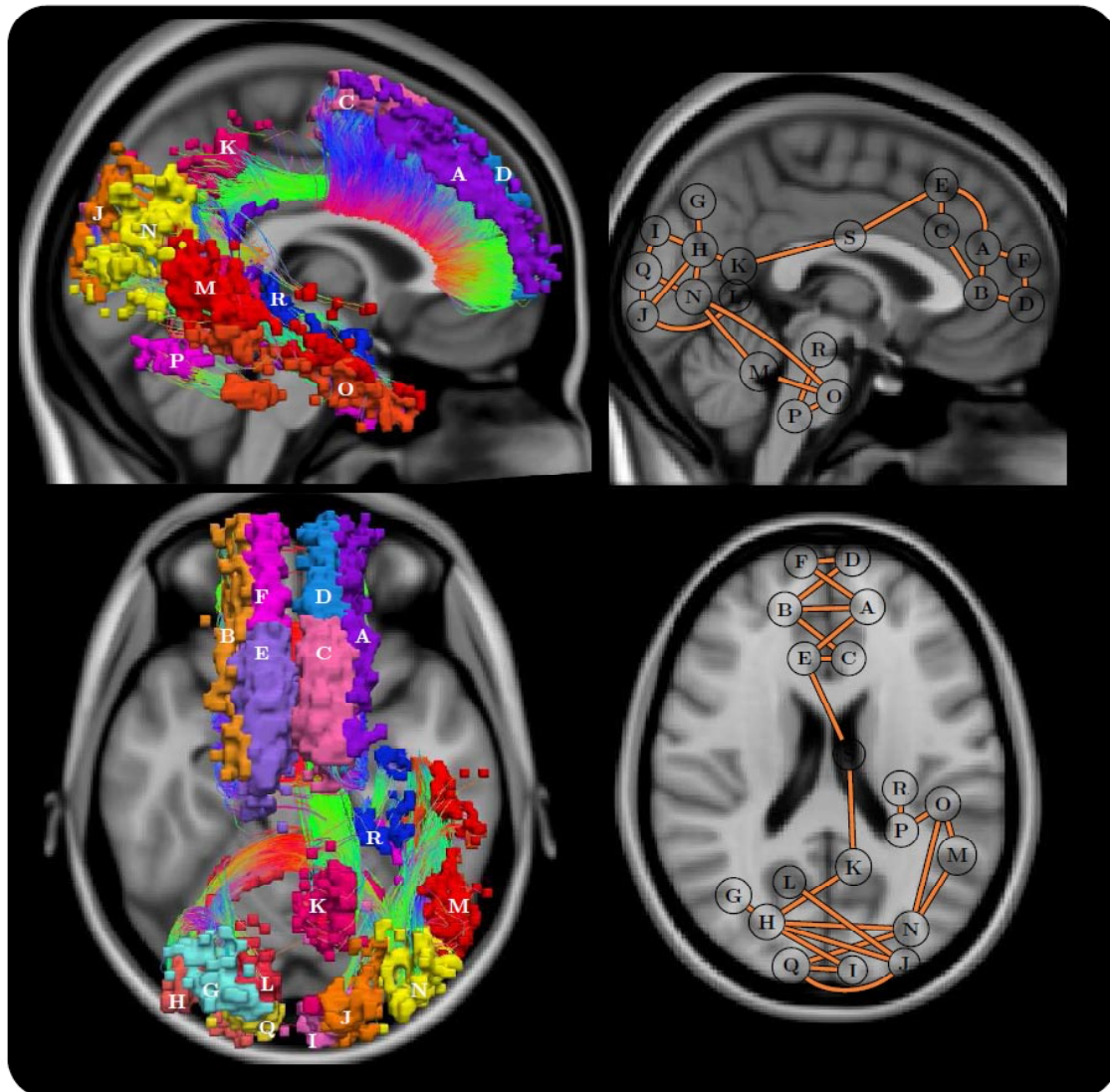
Figure S3. Schematic of the network that was impaired in schizophrenia (*p* = 0.01, corrected), derived using a different set of thresholds than used in Figure 5 (i.e. K_{avg} = 1.5 and a streamline length threshold of 10 mm) . Structures in the left temporal lobe emerged and the frontal subnetwork was augmented to include prefrontal nodes. Left: uniquely colored nodes and streamline representation of interconnecting fiber bundles. Anterior-posterior fibers: green, left-right: red and superior-inferior: blue. Right: planar graph representation, where each node is depicted as a circle positioned at its node's center of gravity. Note that the positioning of some nodes was slightly shifted from the true center of gravity to avert overlapping. Top: sagittal, left hemisphere. Bottom: axial. Node abbreviations: **A**. Left Superior Frontal, **B**. Right Superior Frontal, **C**. Left Supplementary Motor Area, **D**. Left Superior Medial Frontal, **E**. Right Supplementary Motor Area, **F**. Right Superior Medial Frontal, **G**. Right Superior Parietal, **H**.

Right Superior Occipital, **I**. Left Cuneus, **J**. Left Superior Occipital, **K**. Left Precuneus, **L**. Right Precuneus, **M**. Left Middle Temporal, **N**. Left Middle Occipital, **O**. Left Inferior Temporal, **P**. Left Fusiform, **Q**. Right Cuneus, **R**. Left Hippocampus, **S**. Left Middle Cingulum.

1. Mori S (2007): *Introduction to diffusion tensor imaging.* New York: Elsevier.

2. Mori S, Crain BJ, Chacko VP, Van Zijl PC (1999): Three-dimensional tracking of axonal projections in the brain by magnetic resonance imaging. *Ann Neurol.* 45(2):265-269.

3. Tzourio-Mazoyer N, Landeau B, Papathanassiou D, Crivello F, Etard O, Delcroix N, *et al.* (2002): Automated anatomical labeling of activations in SPM using a macroscopic anatomical parcellation of the MNI MRI single-subject brain. *NeuroImage.* 15(1):273-289.

4. Gong G, He Y, Concha L, Lebel C, Gross DW, Evans AC, Beaulieu C (2009): Mapping anatomical connectivity patterns of human cerebral cortex using in vivo diffusion tensor imaging tractography. *Cereb Cortex.* 9:524-536.

5. Bullmore E, Sporns O (2009): Complex brain networks: graph theoretical analysis of structural and functional systems. *Nat Rev Neurosci.* 10:186-198.

6. Rubinov M, Sporns O (2010): Complex network measures of brain connectivity: Uses and interpretations. *Neuroimage.* 52:1059-69.

7. Newman MEJ (2003): The structure and function of complex networks. *SIAM Rev.* 45:167-256.

8. Bassett DS, Bullmore E, Verchinski BA, Mattay VS, Weinberger DR, Meyer-Lindenberg A (2008): Hierarchical organization of human cortical networks in health and schizophrenia. *J Neurosci.* 28(37):9239-9248.

9. Latora V, Marchiori M (2001): Efficient behavior of small-world networks. *Phys Rev Lett.* 87(19):198-701.

10. Watts DJ, Strogatz SH (1998): Collective dynamics of 'small-world' networks. *Nature.* 393:440-442.

11. Maslov S, Sneppen K (2002): Specificity and stability in topology of protein networks. *Science.* 296:910-913.

12. Bullmore ET, Suckling J, Overmeyer J, Rabe-Hesketh S, Taylor E, Brammer MJ (1999): Global, voxel and cluster tests, by theory and permutation, for differences between two groups of structural MR images of the brain. *IEEE Trans Med Imaging.* 18:32-44.

13. Nichols TE, Holmes AP (2001): Nonparametric permutation tests for functional neuroimaging: a primer with examples. *Hum Brain Mapp.* 15:1-25.